Progress In Electromagnetics Research C, Vol. 124, 135–153, 2022

Isolation Analysis of Miniaturized Metamaterial-Based MIMO Antenna for X-Band Radar Applications Using Machine Learning Model

Jyothsna Undrakonda* **and Ratna K. Upadhyayula**

Abstract—A novel metamaterial-based circular patch multi-input multi-output (MIMO) antenna is designed with a 'C'-shaped defected ground structure for high isolation. A $4 \times 4\,\text{mm}^2$ unit cell for a ring resonator has been designed and exhibited double negative material (DNG) properties from 1.0 to 2.92 GHz and 13.68 to 17.67 GHz and Mu negative material (MNG) from 4.70 to 13.67 GHz. The proposed antenna structure is designed by embedding the ring resonator-based meta-structure to a circular patch antenna and fabricated with dimensions $0.245\lambda_0 \times 0.409\lambda_0$ ($15 \times 25\,\text{mm}^2$). The proposed antenna operating at 8.50 to 14.23 GHz for X and lower Ku bands is used in the Unmanned Arial Vehicle (UAV's) applications. The spacing between elements is $0.088\lambda_0$ (5.4 mm) on an FR4 epoxy substrate, and the 'C'-shaped structure on the back of the antenna improves the isolation of more than 24 dB in the operating band. Distance between the antenna elements plays a crucial role, and parameters affected by this are optimized by introducing machine learning. For future predictions, a linear regression model was created to optimize the parameters' linear dependencies like isolation and return loss on the distance between the antenna elements. The radiation efficiency and gain of the antenna are enhanced by 92% and 6.02 dB at 13.22 GHz, respectively. The MIMO antenna's simulated results of diversity and other parameters are in the acceptable range with the measured results used for X-band radar applications. The proposed decoupling technique is simple to understand and implement.

1. INTRODUCTION

Effective 5G communication necessitates higher quality, interference-free data transfer at higher data rates at all times, regardless of weather conditions or signal traffic issues. Radar detects objects, and communication in adverse weather conditions demands more confidential communication systems such as defence applications. Hence, an antenna can handle high data rates with qualitative data transfer even in a worse medium without fading out the data bits. MIMO technology is the array of antennas dedicated to the specified task. The frequency band (i.e., X-band) offers higher data rates irrespective of weather conditions, and MIMO is used in radar applications [1–6]. MIMO antenna design has a limitation that degrades the antenna's performance: mutual coupling. The concept of mutual coupling depends on the spacing between the antenna elements, which decreases with an increase in spacing. Hence, here comes the problem of size, which increases by increasing the space between elements. The techniques to overcome the coupling issue and improve the isolation incorporated parasitic elements, neutralizing lines, stubs, metamaterials, and defected ground structures are discussed in [7]. Near-zero index and epsilon metamaterial are used for a 16-port MIMO antenna system for 5G communications to achieve high isolation and gain discussed in [8]. Metasurface is used for the antenna operated in three bands (X, Ku, and K) and achieves the highest isolation of 32 dB [9]. The defected ground structure

Received 2 August 2022, Accepted 31 August 2022, Scheduled 21 September 2022
* Corresponding author: Jyothsna Undrakonda (jyothsna.1511@gmail.com).
The authors are with the Department of EECE, GITAM Deemed to be University, Visakhapatnam, A.P, India.

used for ultra-wideband (UWB) applications is discussed in [10]. A wideband antenna designed for 5G applications in [11] provides good isolation of −20 dB. A 4×6 defected ground structure array is used in X-band MIMO applications discussed [12]. Metasurface is used for getting multiple operating bands for 5G/WiMAX/WLAN/X-band [13]. Parasitic strips and different electromagnetic band-gap (EBG) structures divert current distribution for WiMAX, WLAN, and X-band applications [14]. Near zero index (NZI) metamaterial is used for high-frequency application with good isolation and gain of 24 dB and 12.4 dBi discussed in [15]. Parasitic decoupling mechanism is used for designing an antenna with 20 dB isolation [16]. A Vivaldi MIMO antenna uses split ring resonator (SRR) for isolation in dual-band applications [17]. Partial and defected ground structure (DGS) structures are used for multi-band operation with an isolation of 22 dB [18]. An L-shaped complementary split ring resonator (CSRR) metamaterial structure-based isolation technique is used for multiband applications with more than 22 dB isolation [19]. Epsilon negative material (ENG) type metamaterial is used as a decoupling technique for 8-port UWB applications [20]. A wearable MIMO antenna uses an EBG structure for isolation with a good gain of 6 dB [21]. An X-shaped isolation block is used to design a 4-port wideband antenna [22]. A mushroom-type EBG structure is utilized for UWB applications [23]. A UWB antenna uses an EBG structure for isolation [24]. An EBG structure is based on the metamaterial used to isolate UWB antenna for X, Ku, K, and Ka-band applications with maximum isolation of 37 dB [25]. A filtenna uses a COVID-19 shaped structure for UWB applications with an isolation of −30 dB [26]. Metamaterial with near zero refractive index (NZRI) and DNG property-based square SRR (SSRR) unit cells is utilized for quad-band applications [27]. Single negative metamaterial (SNG) is used as a decoupling element for UWB applications [28]. A transparent antenna is designed with different substrates for wideband application with the isolation greater than 15 dB [29]. Various techniques are introduced to reduce the mutual coupling effect between radiation elements in an antenna array in MIMO using metasurfaces [30, 31]. Dielectric circles are etched in a cross-shaped microstrip frame and a U-shaped microstrip transmission line to reduce mutual coupling [32, 33]. Decoupling slabs and metasurface-based slots are employed to reduce mutual coupling [34–38]. A metamaterial electromagnetic bandgap structure is used for the reduction in isolation [39]. A fractal isolator, EBG structures, and metamaterial decoupling structure are used in [40, 41].

In this paper, a circular patch MIMO antenna with ring resonators is designed with $0.245\lambda_0 \times 0.409\lambda_0$ ($15 \times 25\,\text{mm}^2$) with a distance between elements $0.088\lambda_0$ (5.4 mm). Despite having a circular patch with the same radiation pattern in all directions, patch antennas have narrow bandwidth and low gain limitations. Using negative index material, i.e., incorporating metamaterial to antenna design, gives an intense improvement in the gain maximum up to 5.9 dB at 13.22 GHz, and the antenna operates at multiple frequencies as the unlicensed bands from 5.1 to 5.3 GHz (for Wi-Fi) and from 8.79 to 14.23 GHz (i.e., X & lower Ku band) which are highly acceptable by both government and military communication and navigation applications, achieving the isolation less than −15 dB. For further isolation improvement, a 'C' shaped block is placed on the antenna's ground face, then an isolation growth is observed from 15 to 20 dB. Further adding 2 and 3 'C' blocks, more observation in isolations is 22 dB and 24 dB, respectively. Finally, we use a 3-slot 'C' shaped defected ground structure in the antenna to get more than 24 dB isolation throughout the operating band and increase the antenna's bandwidth and gain. We achieve the isolation up to 46 dB at 13.22 GHz. By removing the structure, the impact on isolation is investigated through surface current distribution on the antenna.

Machine learning techniques usage have increased because of their fast and efficient nature compared to conventional simulation tools and standard design techniques. The linear regression model gives the most effective relationship between independent and dependent variables through the statistical method. The prediction of values, which are more significant for analysis with this application area, is also improved.

In the paper, Section 2 explains the proposed structure with metamaterial and the mathematical analysis for resonance frequency, and the machine learning model algorithm for isolation analysis based on the distance between antenna elements. Section 3 delivers a brief idea of simulated and measured parameters comparison. The main diversity parameters that describe the MIMO antenna performance are shown in Section 4. Section 5 compares the proposed work with similar existing works. Finally, the conclusions are in Section 6 and followed by acknowledgment.

2. PROPOSED ANTENNA DESIGN METHODOLOGY AND ANALYSIS

The proposed MIMO antenna design steps are shown in Fig. 1. The work starts with designing a metamaterial unit cell (i.e., four ring resonator) and analyzing its properties. Then the final antenna design for the desired frequency band uses meta cell. Finally, the MIMO antenna is designed for the desired band of frequency. The flowchart provides a quick view of the steps for designing the antennas based on metamaterial, and antenna parameters are optimized with the help of a supervised learning model by taking simulated data. With this, predictions of future values for unknown data sets are possible.

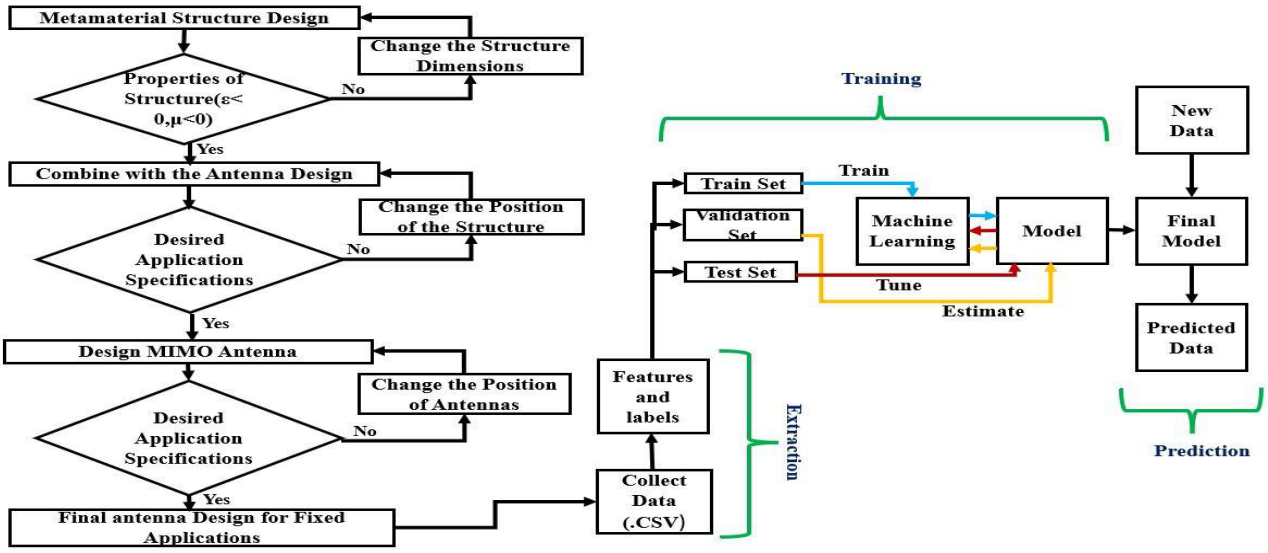

Figure 1. Methodology of the Proposed antenna.

2.1. Metamaterial Antenna Design

2.1.1. Metamaterial Unit Cell Design

Metamaterial gives unique properties such as negative permittivity and negative permeability. Because of these properties, the back wave propagation comes into the role, which diverts the surface current distribution on the antenna. Here, a patch antenna is utilized because of its low profile, easy fabrication, low gain, and narrow bandwidth limitations. Those can be overcome by the simple technique of introducing meta-structure into the antenna design.

For radar applications, detecting the object's direction, position, and range is crucial. We need a low profile & high gain MIMO antenna, which is achieved by taking a circular patch with circular ring resonators. Four ring meta structures of $4 \times 4\,\text{mm}^2$ size are designed with various outer radii of 2.30 mm, 2.82 mm, 3.02 mm, and 3.53 mm. The designed cell is simulated with the HFSS tool, exported to the comma-separated values (CSV) file, and then unit cell parameters are analyzed through the MATLAB tool and Nicolson Ross Weir method. The unit cell satisfies the metamaterial properties shown in Fig. 2. The property of DNG is from 1 to 2.92 GHz and 13.68 to 17.67 GHz. It also acts as mu negative metamaterial (MNG) from 4.70 to 13.67 GHz.

Nicolson-Ross-Weir Method: The assumption of S_{11} & S_{21} parameters, permeability and permittivity are calculated using the metamaterial with the Nicolson-Ross-Weir (NRW) approach by equation [42].

$$\mu_r = \frac{2 \cdot c \cdot (1 - V_1)}{w \cdot d \cdot i(1 + V_2)} \tag{1}$$

$$\in_r = \mu_r + \frac{2 \cdot S_{11} \cdot c \cdot i}{w \cdot d} \tag{2}$$

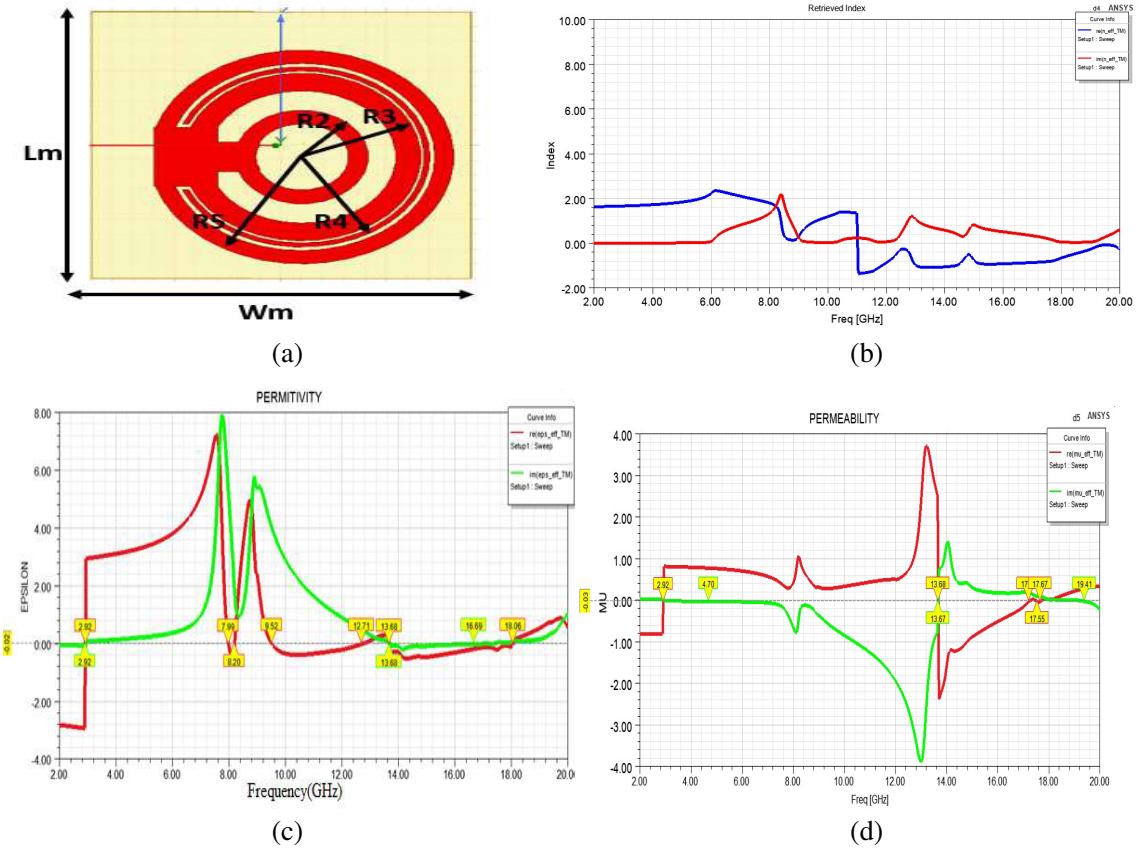

Figure 2. Unit cell, (a) metamaterial structure, (b) index, (c) permittivity, (d) permeability.

$$V_1 = S_{11} + S_{21} \tag{3}$$

$$V_2 = S_{21} - S_{11} \tag{4}$$

where w = frequency in radiation, V_1 = voltage maxima, c = speed of light/vacuum, V_2 = voltage minima, d = substrate thickness.

2.1.2. Antenna Design

The circular patch obtains the radiation pattern uniformly all over the operating band. A circular patch of a radius of 0.85 mm is designed and fed with a 50 Ohm microstrip line on an FR4 epoxy substrate of a thickness of 1.6 mm. The following equations are used to create the patch, as discussed in [43].

$$a = \frac{F}{\left\{1 + \frac{2h}{\pi\varepsilon_r F}\left[\ln\ln\left[\frac{\pi F}{2h}\right] + 1.7726\right]\right\}^{\frac{1}{2}}} \tag{5}$$

$$F = \frac{8.791 \times 10^9}{f_r\sqrt{\varepsilon_r}} \tag{6}$$

$$\varepsilon_{eff} = \frac{1}{2}(\varepsilon_r + 1) + \frac{1}{4}\frac{(\varepsilon_r - 1)}{\sqrt{1 + \frac{12h}{a}}} \tag{7}$$

$$a_r = \frac{1.8412\,c}{2\pi f_r\sqrt{\varepsilon_r}} \tag{8}$$

2.1.3. Mathematical Analysis through Equivalent Circuit

The proposed antenna is designed by placing the metamaterial structure near the circular patch. The proposed system achieves multiple operating frequencies from 5.02 to 5.13 GHz, 7.74 to 7.96 GHz, and 9.25 to 14.06 GHz, with the highest return loss of −35 dB at 10.83 GHz. The antenna's gain and radiation efficiency are above 5.5 dB & 94%, respectively. The designed metamaterial-based circular patch antenna is analyzed through an equivalent circuit simulated in ADS software shown in Fig. 3 [44]. Here the term 'Cc' indicates the coupling capacitor. Ring resonators are joined together in a series. Then there is an effect of coupling or mutual interactions balanced by the parallel combination of 'Lc' & 'Cc' (Coupling capacitor& inductor) connected in each ring circuit shown in Fig. 3.

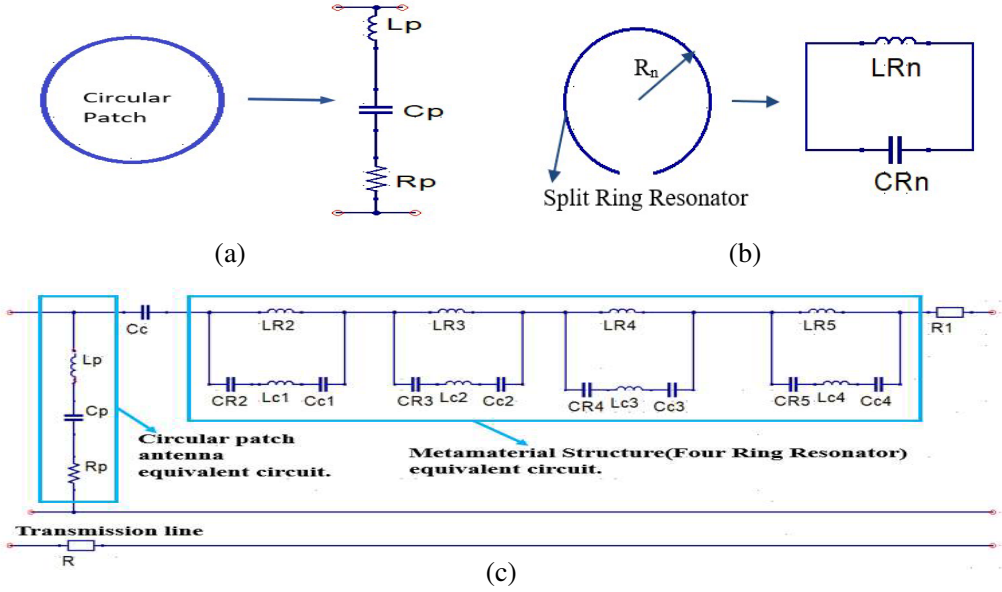

Figure 3. Equivalent circuit, (a) circular patch, (b) split-ring resonator, (c) overall equivalent circuit.

The resonance frequencies are,

$$F_z^2 = \frac{1}{2\Pi\sqrt{LR_2CR_2}}, \quad F_z^3 = \frac{1}{2\Pi\sqrt{LR_3CR_3}}, \quad F_z^4 = \frac{1}{2\Pi\sqrt{LR_4CR_4}}, \quad F_z^5 = \frac{1}{2\Pi\sqrt{LR_5CR_5}}$$

$$F_{z1} = \frac{1}{2\pi}\sqrt{\frac{CR_2 + Cc_1}{Cc_1CR_2\,(Lc_1 + LR_2)}}, \quad F_{z2} = \frac{1}{2\pi}\sqrt{\frac{CR_3 + Cc_2}{Cc_2CR_3\,(Lc_2 + LR_3)}}$$

$$F_{z3} = \frac{1}{2\pi}\sqrt{\frac{CR_4 + Cc_3}{Cc_3CR_4\,(Lc_3 + LR_4)}}, \quad F_{z4} = \frac{1}{2\pi}\sqrt{\frac{CR_5 + Cc_4}{Cc_4CR_5\,(Lc_4 + LR_5)}}$$

$$F_M = \frac{1}{2\pi\sqrt{\left(L_{eq} + \left[\left(\frac{Lt_1}{Lt_2}\right)\left(\frac{Ct_1}{Ct_2}\right)\right] + \left[\left(\frac{Lt_3}{Lt_4}\right)\left(\frac{Ct_3}{Ct_4}\right)\right] + \left[\left(\frac{Lt_5}{Lt_6}\right)\left(\frac{Ct_5}{Ct_6}\right)\right]\right)}} \tag{9}$$

$$\begin{aligned}
[L_{t1} &= LR_2LR_3 + LR_3Lc_2 + LR_3Lc_1 + Lc_1Lc_2, \quad L_{t3} = LR_3LR_4 + LR_3Lc_3 + LR_4Lc_2 + Lc_2Lc_3,\\
L_{t5} &= LR_4LR_5 + LR_5Lc_4 + LR_5Lc_3 + Lc_3Lc_4, \quad L_{t2} = LR_2 + LR_3 + Lc_2 + Lc_1,\\
L_{t4} &= LR_3 + LR_4 + Lc_3 + Lc_2, \quad L_{t6} = LR_4 + LR_5 + Lc_3 + Lc_4,\\
C_{t1} &= CR_2CR_3CR_1 + CR_2Cc_2Cc_1 + CR_2Cc_2CR_3 + Cc_1CR_3Cc_2,\\
C_{t2} &= CR_2CR_3 + CR_2Cc_2 + Cc_1CR_3 + Cc_1Cc_2,\\
C_{t3} &= CR_2Cc_2CR_4 + CR_2Cc_2Cc_3 + CR_4Cc_3CR_3 + Cc_2CR_4Cc_3,
\end{aligned}$$

$$Ct_4 = CR_3CR_4 + CR_3Cc_3 + Cc_2CR_4 + Cc_2Cc_3,$$
$$C_{t5} = CR_4Cc_3CR_5 + CR_4Cc_4Cc_3 + CR_4Cc_4CR_5 + Cc_3CR_5Cc_4,$$
$$C_{t6} = CR_4CR_5 + CR_4Cc_4 + Cc_3CR_5 + Cc_3Cc_4]$$

The proposed antenna manufacturing circuit is designed by considering the values of circuit components as $LR_2 = 0.005\,\text{nH}$, $LR_3 = 6.58\,\text{nH}$, $LR_4 = 5.4008\,\text{nH}$, $LR_5 = 1.90405\,\text{nH}$, $Lc_1 = 12.66\,\text{nH}$, $Lc_2 = 0.1696\,\text{nH}$, $Lc_3 = 0.01550\,\text{nH}$, $Lc_4 = 10.680\,\text{nH}$, $CR_2 = 10.6635\,\text{pF}$, $CR_3 = 3.105\,\text{pF}$, $CR_4 = 0.09645\,\text{pF}$, $CR_5 = 3.9207\,\text{pF}$, $Cc_1 = 12.66\,\text{pF}$, $Cc_2 = 0.001\,\text{pf}$, $Cc_3 = 4.702321\,\text{pF}$, $Cc_4 = 0.15099\,\text{pF}$ and L_{eq} equivalent of transmission line inductance. With this, we have achieved the resonance frequency of the metamaterial equivalent circuit $F_{.M.} = 6.267\,\text{GHz}$. The patch equivalent circuit frequency can be written as,

$$F_p = \frac{1}{2\pi\sqrt{\left(L_p + \left[\left(\frac{C_P C_C}{C_P + C_C}\right)\right]\right)}} \tag{10}$$

Considering the approximate inductance and capacitance values, the antenna is resonant at 7.097 GHz. Half power frequencies in the series LCR circuit are $F_{.M.}$ & $F_{.P.}$ finally. The proposed antenna resonates at 9.39 GHz, in the frequency band of 8.50 to 14.23 GHz.

2.2. MIMO Antenna Design

The proposed MIMO antenna design is shown in Fig. 4. It comprises two circular patch antennas with four ring resonators and a 'C' shaped defected ground structure of $9 \times 2\,\text{mm}^2$ dimensions. The proposed antenna is designed on the readily available low-cost FR4 epoxy with thickness of 1.6 mm, tangent loss of 0.02, and dielectric constant 4.4 using HFSS 2020 R2. The designed antenna is fabricated with

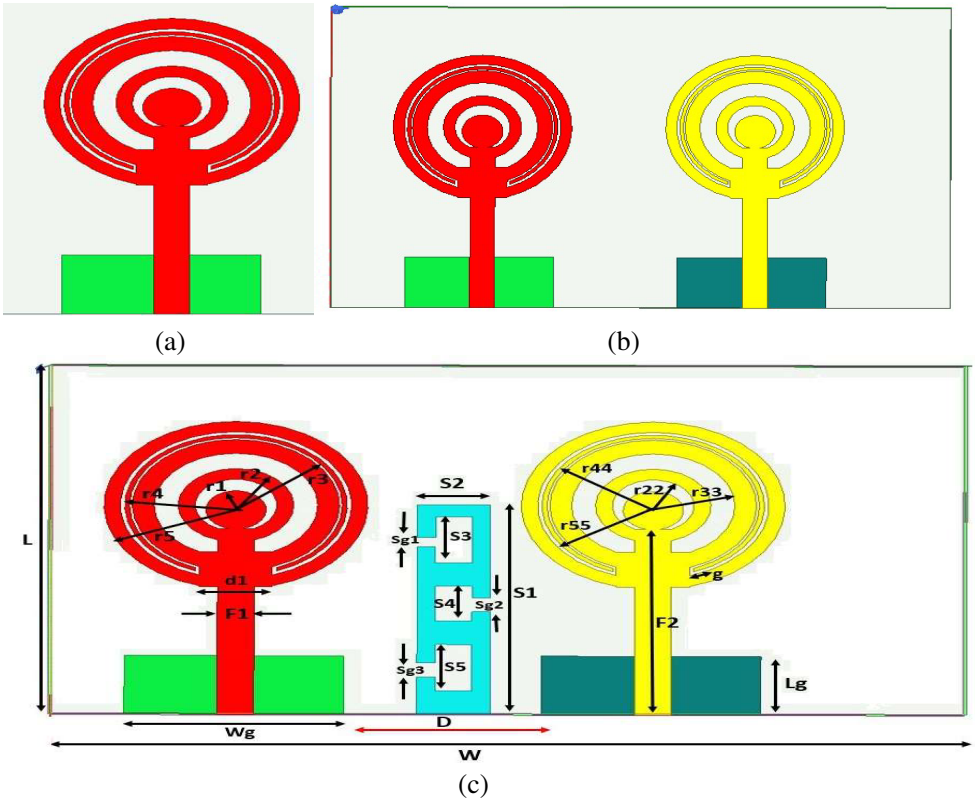

Figure 4. Antenna model design, (a) SISO, (b) MIMO without structure, & (c) MIMO with structure.

dimensions $15 \times 25\,\text{mm}^2$ with 5.4 mm as the distance between the antenna elements. The partial ground is incorporated for the back lobe reduction of the microstrip patch antenna by decreasing the surface wave distribution from the antenna ground plane. All the dimensional parameters of the structure are noted in Table 1.

Table 1. Dimensions of antenna parameters.

Parameter	Value (mm)	Parameter	Value (mm)
L	15	r_1	0.85
W	25	r_2	2.30
Lg	2.5	r_{22}	1.717
Wg	6	r_3	2.82
F_1	1	r_{33}	2.25
F_2	8.10	r_4	3.02
g	0.14	r_{44}	2.94
D	5.4	r_5	3.53
S_1	9	r_{55}	3.12
S_2	2	S_3	2
S_4	1.5	S_5	2
Sg_1	0.4	Sg_2	0.6
d_1	2	Sg_3	0.6
Lm	4	Wm	4

2.2.1. Antenna Design Steps

The design steps are clearly shown in Fig. 4. First step: A four-ring resonator-based circular patch antenna is designed. Single SISO antenna gives three bands, 5.02 to 5.13 GHz, 7.74 to 7.96 GHz, and 9.25 to 14.06 GHz. These are not under the required band of frequencies. Second step: one more antenna is positioned at distances D of 4.4 mm, 5 mm, 5.4 mm, 7 mm, and 8 mm. When $D = 7$ & 8 mm, isolation nearly equal to 10 dB is noticed. When $D = 4$ & 5 mm good return loss is exhibited above -40 dB with isolation nearly equal to 15 dB. If $D = 5.4$ mm, the antenna operates at frequency band 8.50 to 14.23 GHz with a return loss of -25 dB but with isolation above 15 dB throughout resonating band.

The S parameters (S_{11} & S_{21}) variations of two antennas at 4.4 mm, 5 mm, 5.4 mm, 7 mm, & 8 mm are shown in Fig. 5(a) at $D = 5.4$ mm, and the isolation is above 15 dB and up to 17 dB. A 'C' structure is introduced at the bottom of the antenna for further isolation, and it is noticed that the isolation improves above 24 dB mostly (95%) all over the operating band. Fig. 5 represents the bandwidth (S_{11}) performance for Single Input Single Output (SISO) and MIMO antenna designs without and with a 'C' type DFG structure.

2.3. Parametric Analysis

2.3.1. Effect of Ground Length and Width on Isolation

Ground length Lg and Wg show significant variation in return loss at different operating frequencies while varying by $Lg = 2.5$ mm, 1 mm, 2.2 mm, 1.4 mm & 1.8 mm, and $Wg = 4.4$ mm, 5 mm, 5.6 mm, and 6 mm. Most of the values got the same frequency band with different resonance frequencies, for 2.2 mm, four narrow bands with isolation below 15 dB. At $Lg = 2.5$ mm and $Wg = 6$ mm, the antenna operated at acceptable bars from 8.50 to 14.23 GHz with high isolation compared to the remaining lengths. It is clearly shown in Fig. 6(a).

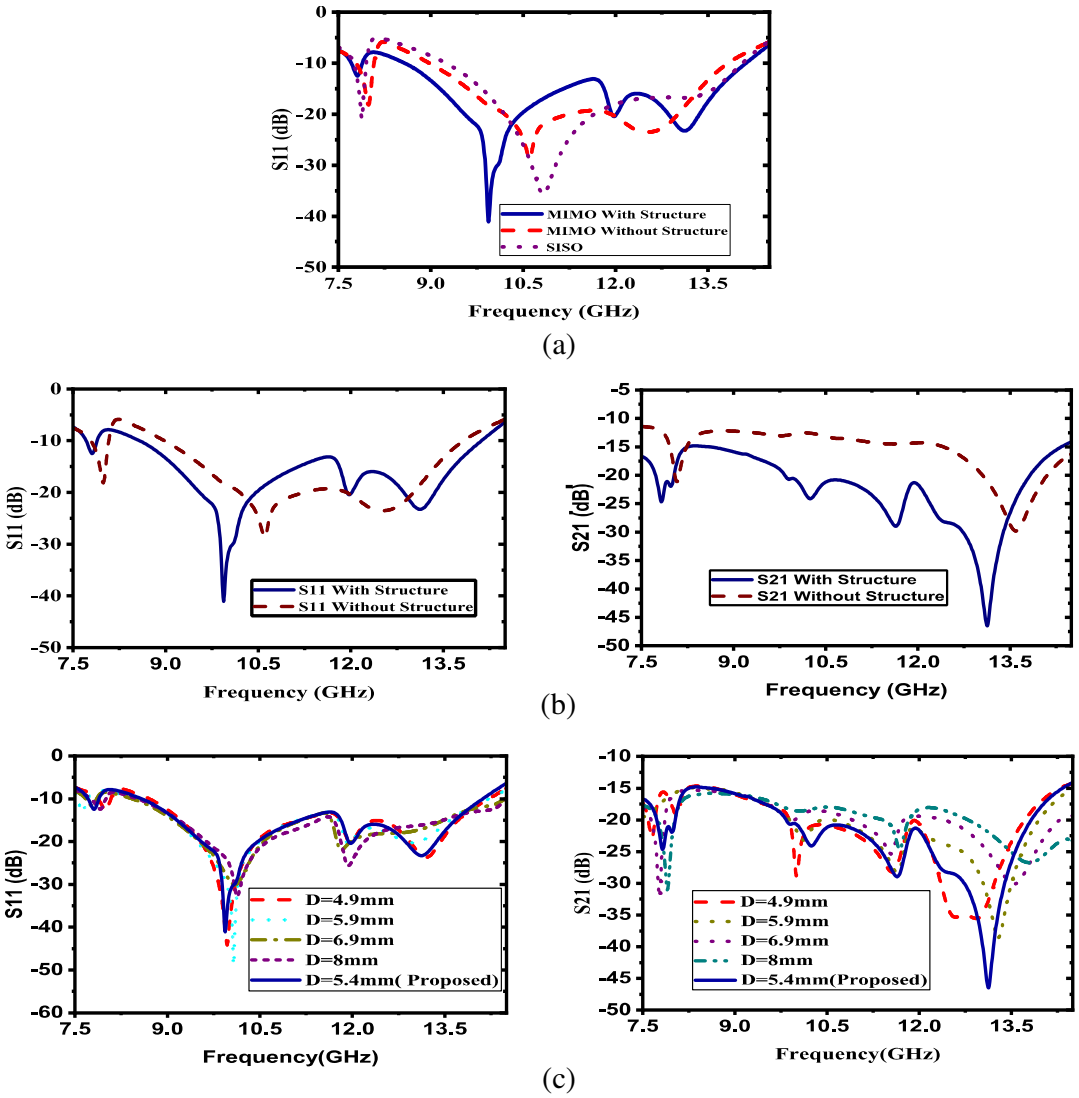

Figure 5. Effect of parameters on bandwidth and isolation, (a) SISO & MIMO, (b) with & without structure, (c) distance 'D' between elements.

2.3.2. Effect of Width Transformation of the Antenna on Isolation

The width of the antenna also made a noticeable impact on the return loss at lower resonance frequencies. At $W = 20$ mm, the highest return loss was -60 dB at 10 GHz with variable isolation throughout the band. At $W = 25$ mm, a dual-frequency band was observed with good isolation up to 46 dB at 13.22 GHz. The variation of W with the S parameters is shown in Fig. 6(b).

2.4. Surface Current Analysis

The impact of the 'C' shaped defected structure on the mutual coupling is briefly investigated by surface current distributions on the exciting antenna. Fig. 7 displays the current distribution at frequencies 10.17 GHz, 11.96 GHz, 12.45 GHz, and 13.22 GHz. It is noticed that without structure, there is more impact of mutual coupling on another outer antenna ring and at the feeding line, which matches with the impedance at 50 Ω. Adding the structure on the ground plane removes the mutual coupling effect. Acting as a reflector and storage element reflects the current from one port to the other. 'C' structure mainly acted as a significant obstacle to the mutual coupling impact from the excited antenna to the

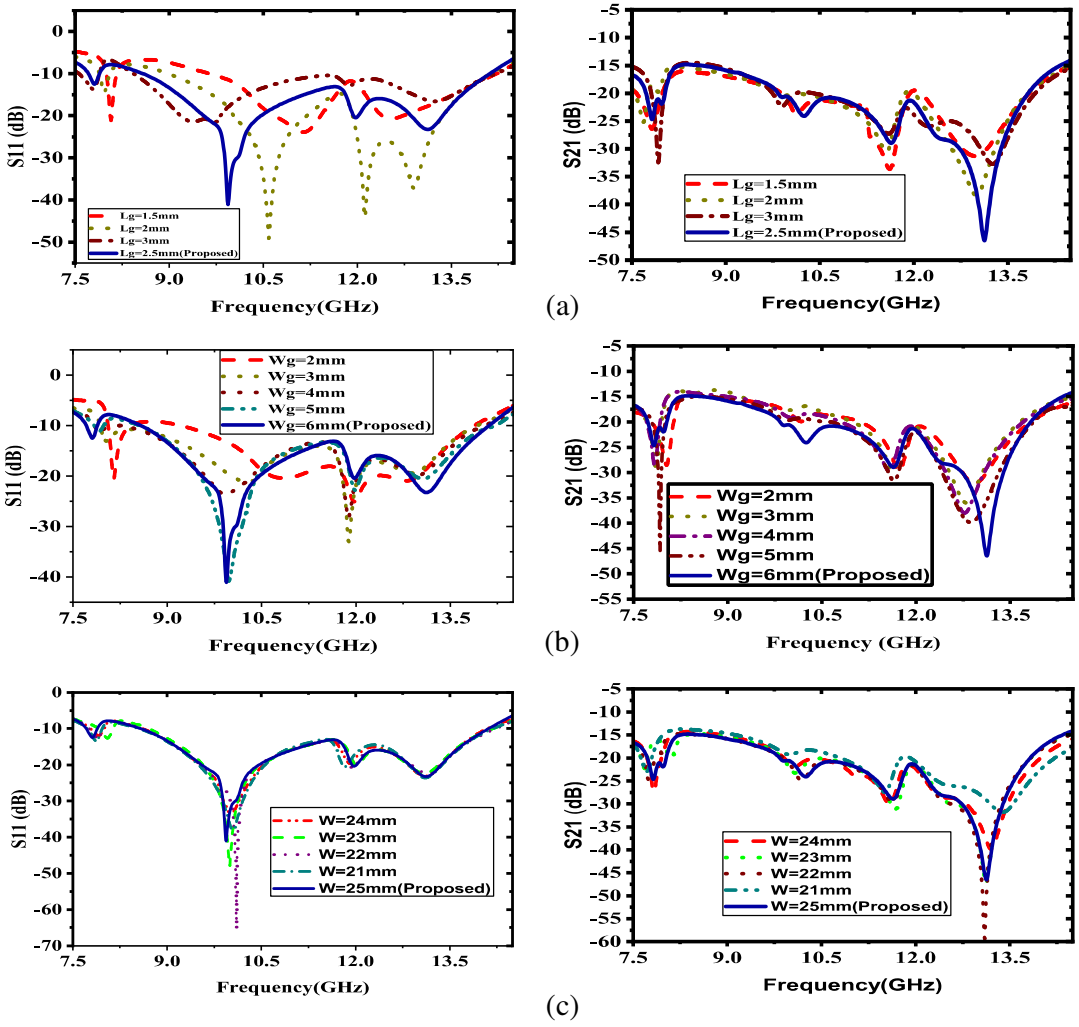

Figure 6. Parametric analysis with S_{11} & S_{21}, (a) & (b) ground length and width variation, (c) antenna width variation.

other. At frequencies 10.17 GHz, 11.96 GHz, and 13.22 GHz, first element coupling has a small effect with isolation of −18 dB, 20 dB, and 23 dB, respectively. At 13.22 GHz, the impact of the exciting antenna is negligible compared to other frequencies with an isolation maximum up to −60 dB.

2.5. Machine Learning (Linear Regression Algorithm)

It is possible to design a relational model using the machine learning technique. From that, it was easy to predict output for any data point instead of only aiming at the available minimum points. This model has broad applicability and allows us to understand the strength of the relationship between variables.

The linear regression algorithm is the part of machine learning (ML) in which the precise relationship between input (independent variable) and output (dependent variable) is represented by a line in space. It was used for continuous variable parameters in the form of numerical data.

The distance between the antenna elements decides the isolation of the antenna. Increase in mutual coupling of the antenna leads to the degradation in the antenna efficiency and correlation with low isolation. So, with a rapid change in the distance between antenna elements, observe the return loss (S_{11}) and isolation (S_{21}). To develop the linear regression model shown in Fig. 8, the distance between antenna (D) elements was used as the independent variable (input) and S_{11} & S_{21} as the dependent variable (output). It is assessed using the Root Mean Square Error (RMSE) and R2 values, which show

how well the model is fitted and how much error there is between the actual and predicted numbers.

$$M = \frac{\Sigma(x - \bar{x})(y - \bar{y})}{\Sigma(x - \bar{x})^2} \tag{11}$$

Here, M = mean, x = input, $\bar{x}$ = mean of input values, y = output, $\bar{y}$ = mean of output values

$$y = mx + c \Rightarrow c = y - mx \tag{12}$$

where 'c' is constant

$$y_p = mx + c \tag{13}$$

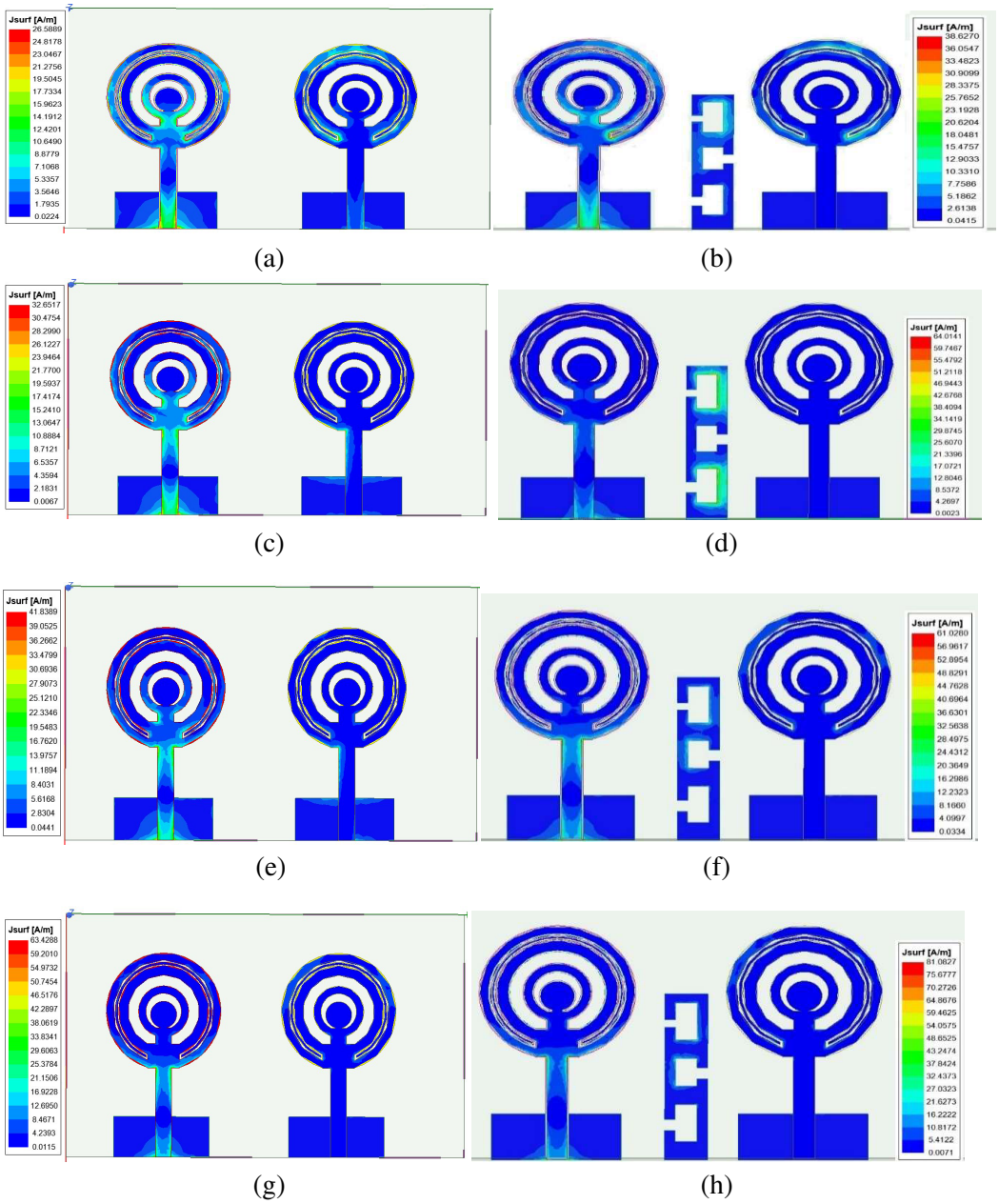

Figure 7. Surface current distribution with & without structure, (a) & (b) at 9.94 GHz, (c) & (d) at 11.97 GHz, (e) & (f) at 12.45 GHz, (g) & (h) at 13.22 GHz.

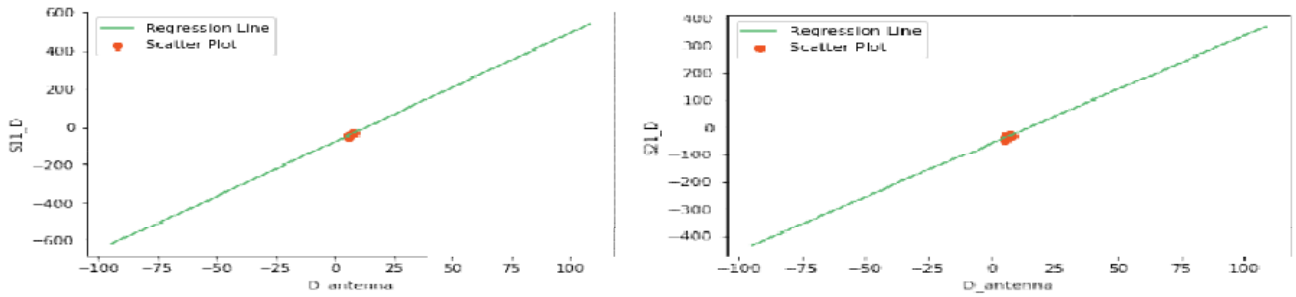

(a) (b)

Figure 8. Linear regression model plot, (a) D vs. S_{11}, (b) D vs. S_{21}.

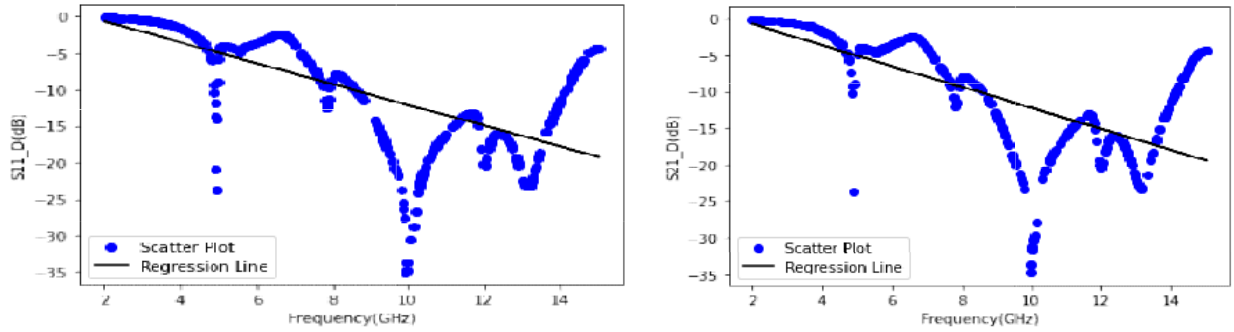

(a) (b)

Figure 9. Linear Regression model using .CSV file, (a) Frequency (GHz) vs S_{11} (dB), (b) Frequency (GHz) vs S_{21} (dB).

where y_p is the predicted output

$$R^2 = \frac{\Sigma\left(y_p - \bar{y}\right)^2}{\Sigma\left(y - \bar{y}\right)^2} \tag{14}$$

From these equations, the value of RMSE is derived, and based on that, it is clear how the model predicted values with error compared to the actual one. Here comes the precise relationship between D & S_{11}, S_{21} with this, which might be accessible to predict the change in S_{11} & S_{21} concerning D. Figs. 8(a) & (b) give a clear view of how accurately the values are fitted to the regression line.

Three more models are also designed using the data (.CSV) collected from the optimetrics in HFSS for the independent variables as frequency (GHz) with dependent variables S_{11} & S_{21} (dB) by keeping the ground length of the antenna (Lg), antenna width (W), and distance between the antenna elements (D) as fixed values for the individual model. This prediction of return loss and isolation of the antenna with respect to frequency at different points becomes easy. Figs. 9(a) & (b) represent the linear regression model, which gives the relationship between the independent variable (Frequency) and the dependent variable (S_{11} & S_{21}).

3. SIMULATED AND MEASURED RESULTS ANALYSIS

3.1. Impedance Analysis

The proposed metamaterial circular patch antenna is designed and fabricated on an FR4 epoxy substrate shown in Fig. 10. It is tested with a network analyzer, and the results, such as return losses and VSWR, are analyzed.

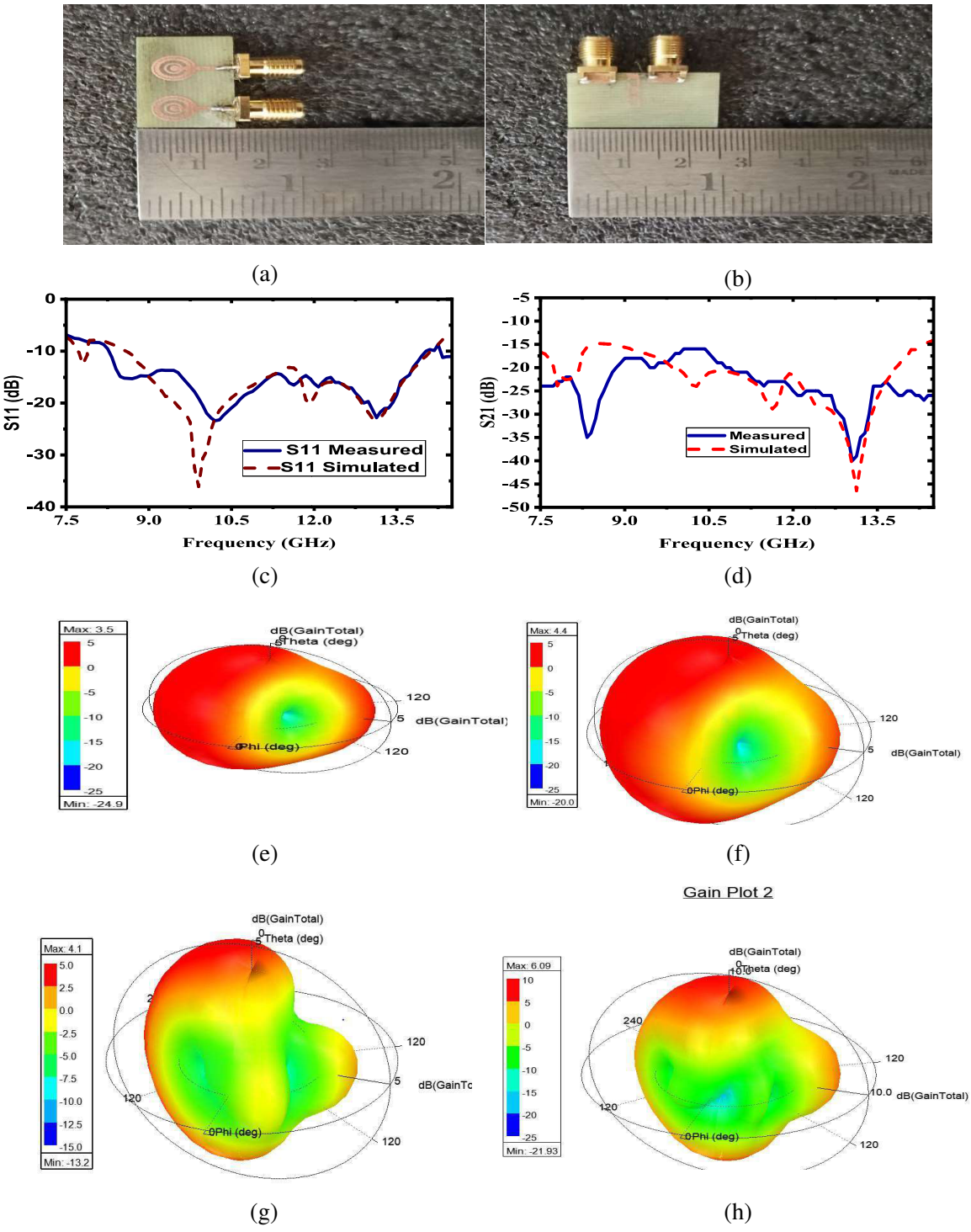

Figure 10. Fabricated antenna with S parameters measured and simulated, (a) front view, (b) bottom view, (c) S_{11}, (d) S_{21} and realized gain at (e) 9.94 GHz, (f) 10.44 GHz, (g) 11.97 GHz, & (h) 13.22 GHz.

It is observed that the simulated and measured results are in acceptable deviation within the frequency band and provide good isolation between the antenna elements. For the bandwidth of 5.44 GHz (8.79–14.23 GHz), the observed isolation value is > 24 dB for the MIMO antenna. Measured results exhibit a bandwidth 5.75 GHz with isolation more significant than 22 dB all over the resonating band.

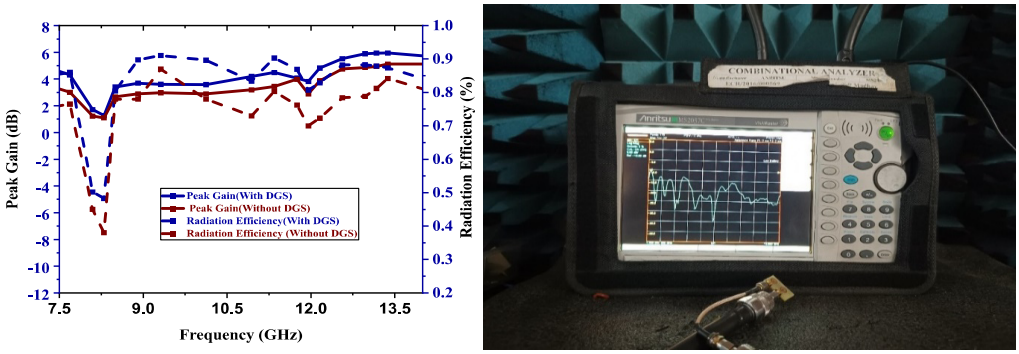
Peak Gain (dB)
Radiation Efficiency (%)
Frequency (GHz)
Peak Gain(With DGS)
Peak Gain(Without DGS)
Radiation Efficiency(With DGS)
Radiation Efficiency (Without DGS)

(a)

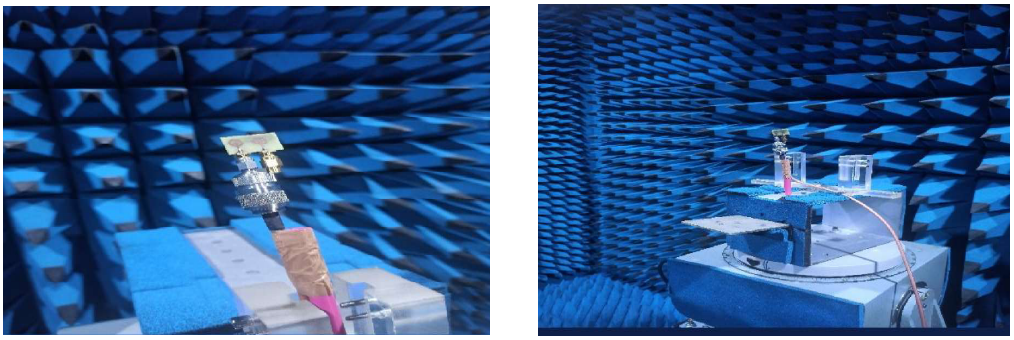

(b)

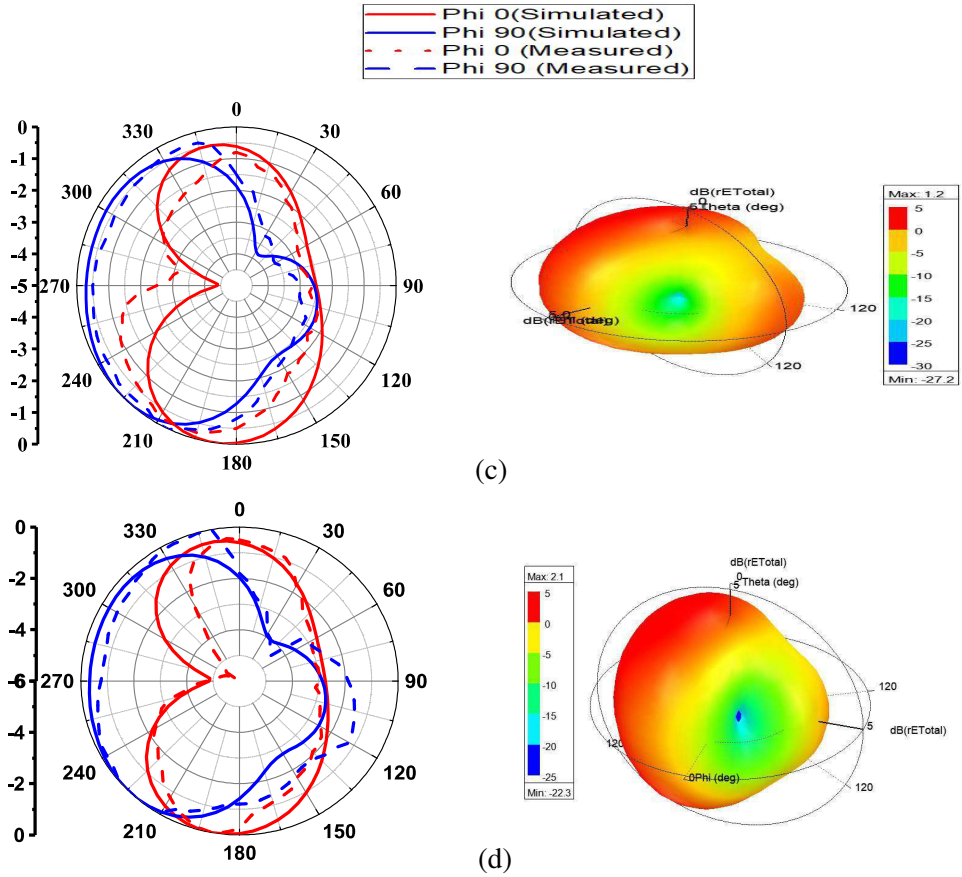
Phi 0(Simulated)
Phi 90(Simulated)
Phi 0 (Measured)
Phi 90 (Measured)
dB(rETotal)
Theta (deg)
Max: 1.2
Min: -27.2
Max: 2.1
Min: -22.3
Phi (deg)

(c)

(d)

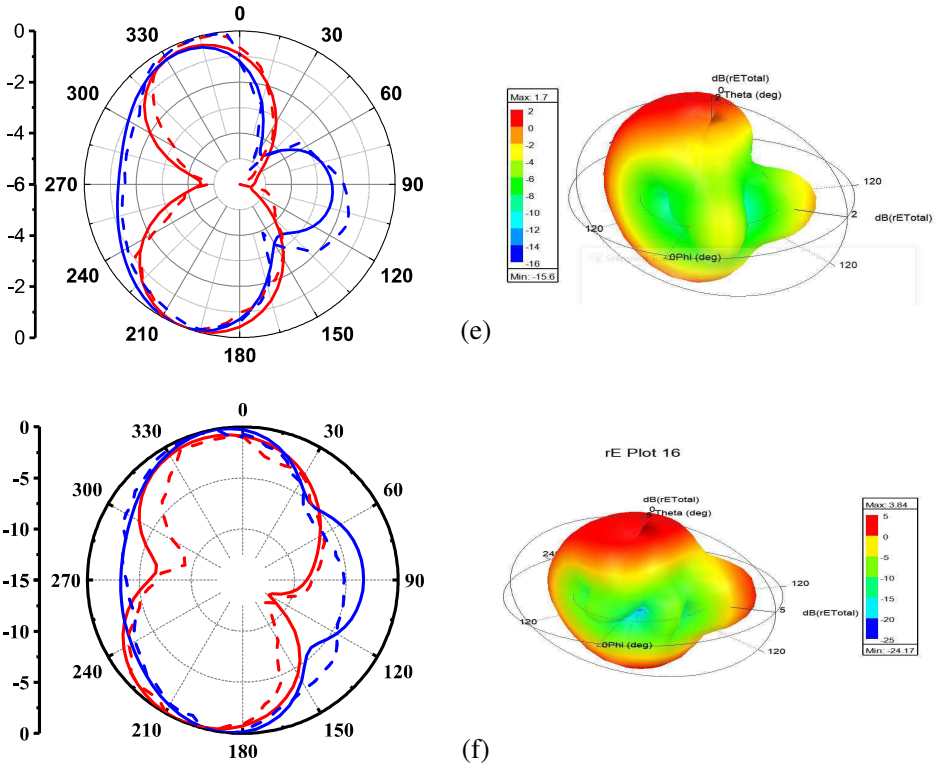

Figure 11. (a) Radiation efficiency and peak gain with and without DGS & Vector analyzer testing, (b) Anechoic chamber testing, (c) 2D & 3D radiation pattern 9.94 GHz, (d) 10.16 GHz, (e) 12.15 GHz, and (f) 13.22 GHz and anechoic chamber antenna photos.

3.2. Radiation Performance

2D & 3D radiation patterns are displayed in Fig. 11. The E and H fields show the isotropic and bidirectional nature pattern. Quiet disturbance was observed in the radiation pattern at different frequencies in the specified band because distortion occurred in the electric field distribution.

The peak gain of the antenna varied from 4.8 dB to 6.0 dB with 0.5 dB steps, and the maximum gain of 6.02 dB was observed at 13.22 GHz. Efficiency was also observed at more than 91% all over the band, and the max efficiency was observed at 9.27 GHz. Directivity also improved with the final antenna design. Peak gain and radiation efficiency with and without Defected Ground Structure (DGS) in between radiation elements variation clearly shown in Fig. 11(a).

4. DIVERSITY PARAMETER ANALYSIS FOR MIMO

The proposed MIMO antenna performance is analyzed through five parameters: envelope correlation coefficient (ECC), diversity gain (DG), mean effective gain (MEG), channel capacity loss (CCL), & the total active reflection coefficient (TRAC). The envelope correlation coefficient describes the correlation between antenna elements. Different correlations existed between two or more connected antenna elements: power, signal, and envelope correlations. Signal correlation gives the equality of signals to generate a new signal. Power correlation is counted by the square of magnitude signal equal to the envelope correlation. ECC is another key parameter to define mutual coupling between elements, directly proportional to radiating elements. ECC value is considered between 0 & 1, but practically below 0.5 is acceptable. In this work, it is considered below 0.1, measured through the S-parameters technique [45], and Eq. (15) is used to measure this value. Alternate methods to measure ECC are far-field radiation pattern, an S-parameter, and radiation efficiency. DG is also an important parameter to describe the compatibility of both antenna signals combined to give an output signal, and the formulated

is Eq. (16).

$$ECC = \frac{|S_{11}^* S_{12} + S_{21}^* S_{22}|^2}{\left(1 - |S_{11}|^2 - |S_{21}|^2\right)\left(1 - |S_{22}|^2 - |S_{12}|^2\right)} \tag{15}$$

$$DG = 10\sqrt{1 - ECC^2} \tag{16}$$

$$TARC = \sqrt{\frac{(S_{11} + S_{12})^2 + (S_{22} + S_{21})^2}{2}} \tag{17}$$

$$C_{LOSS} = -\log_2 |\varphi^R| \tag{18}$$

$$MEG = \frac{mean\ received\ power}{total\ mean\ received\ power} \tag{19}$$

The gain is measured as 9.953 dB. The ECC and DG are represented in Fig. 12. S_{11} represents the reflected signal. TRAC is described by the ratio of reflected power to incident power. TARC depends on the isolation between the elements, i.e., when isolation is high, the incident signal is transmitted without any loss, less than 10 dB, and the formula calculates TARC in Eq. (17). CCL will give the overall quality of the transmitted signal. This is measured through the data transfer rate through the operating band which is below 0.5 bits/sec/Hz. The proposed MIMO antenna's value is 0.35 bits/sec/Hz, calculated using Eq. (18). Individual antenna's MEG is examined when it is exposed to the environment. The measured value is below 3 dB using Eq. (19).

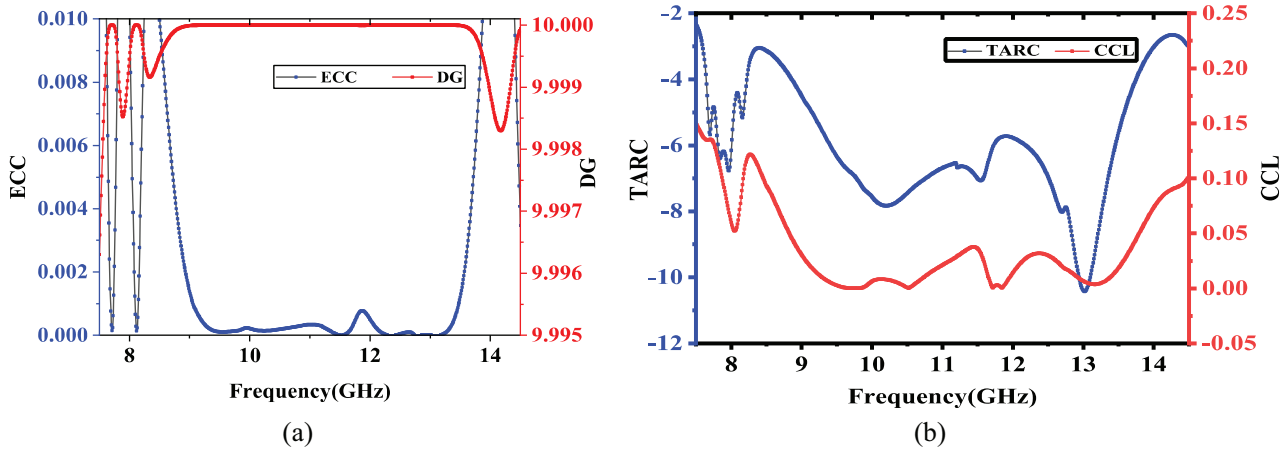

Figure 12. Simulated & Measured, (a) ECC & DG, (b) CCL & TARC.

5. COMPARISON OF PROPOSED DESIGN WITH OTHER

A comparison of extracted parameters such as electrical size, isolation ($S_{21} < -15$ dB), gain, and bandwidth with a similar kind of work is presented in Table 2. It is observed that the highlights of our work on the antenna size are very compact and simple to design with high isolation, low CCL, low ECC, acceptable MEG and TRAC, and high gain. The proposed work was compared to the references [8, 20, 25, 28], which used metamaterial and defected ground structures as the isolation technique achieved the isolation of > 24 dB, a gain of 6.02 dB, and radiation efficiency $> 91\%$ in the entire band.

Table 2. Comparison of proposed work with the existing works.

S. NO	Ref. No & year	Dimensions (mm^2)	Operating Band (GHz)	Isolation (dB)	Isolation Technique	Peak gain (dB)
1.	[8], 2020	22×20	3.35–3.65 (5G)	28	NZI-ENG Metamaterial	6.5
2.	[9], 2019	62.75×0.75	X, Ku & K bands	32, 27 & 26	Meta surface	-
3.	[10], 2018	26×31	3.1–10.6 GHz	20	Defected ground Structure	2.5–5.54
4.	[11], 2019	126×126	24–39 GHz (Ka band)	20	9×9 Array structure	-
5.	[12], 2018	77×79	X, Ku-band	> 15	4×6 Defected ground structure	14.1 & 11.2
6.	[13], 2018	60×60	3.1–6.2, 7.1–8.7	> 15	Meta surface	6 & 8.9
7.	[14], 2021	34×34	3.3–3.9, 5.6, 7.4–8.85	> 15	Parastric strip & C, L, H shaped EBG structure	2.5–5.5
8.	[15], 2020	52×23	24–30	24	NZI Metamaterial	12.4
9.	[16], 2019	40×43	3.1–10.6	20	Parastric	4
10.	[17], 2019	26×26	2.9–11.6	16	SRR	-
11.	[18], 2019	39×39	2.30–13.75	22	Partial & DFG	1.4–4.6
12.	[19], 2020	56×56	1.3–40	> 22	L shaped SRR	-
13.	[20], 2020	28×23	3.1–10.6	20	ENG Metamaterial	-
14.	[21], 2019	-	24	-	EBG	6
15.	[22], 2021	129.5×129.5	1.55–6	16	X-shaped isolation block	-
16.	[23], 2018	64×45	3.3–3.6, 5–6, 7.1–7.9	15	Mushroom EBG	-
17.	[24], 2021	26×31	3.1–11	25	Ground stub & EBG	5.67
18.	[25], 2019	23×23	8.7–11.7, 11.9–14.6, 15.6–17.1, 22–26, 29–34.2	37, 21, 20 & 31	EBG based Metamaterial	-
19.	[26], 2022	50×50	3.3–60	30	Covid-19 shaped	5
20.	[27], 2020	73.6×42.5	2.51–4.324, 4.92–6.49	15	SSRR (NZRI & DNG Metamaterial)	6
21.	[28], 2020	22.5×14	3.08–14.1	15	SNG Metamaterial	4.54
22.	[31], 2021	40×40	8.2–12	> 15	Metasurface	8.5
23.	[34], 2018	25×20	X, Ku & K	26.7 & > 15	Decoupling Slab	Varies b/w 4.2–8.2
24.	[38], 2018	20×30	X, Ku, K & Ka	> 15	Metasurface square wave slot Pattern	Improved 2
25.	[40], 2019	23×23	X, Ku, K & Ka	37, 21, 20 & 31	Fractal isolator & EBG	71% improved
26.	Proposed	15×25	8.50–14.23	24	Metamaterial (DNG & MNG) and DFG	6.02

6. CONCLUSION

A miniaturized metamaterial-based MIMO antenna with a defective ground structure is designed, fabricated, and tested. Four ring resonators in the design enhanced the gain & bandwidth of the circular patch antenna with isolation of 18 dB. A 'C' shaped structure was used to improve the isolation further and achieved a significant isolation improvement up to 24 dB. Peak gain and efficiency values are measured as 6.02 dB and $> 91\%$, respectively, over the entire band. The measured diversity parameters are ECC below 0.010 & DG as 9.953 dB. Miniaturization of antenna is enhanced above 62% compared to previous works. The utilization of a machine learning algorithm, relation model with minimum RMSE, R^2 value above 0.6, and correlation between the antenna parameters achieved above 80% designed to predict the output for any data point is possible. This enables rapid analysis of crucial MIMO parameters such as the distance between antenna elements and isolation range. This MIMO antenna may be used in UAVs & X-Radar systems with frequency bands 8.50 to 14.23 GHz with low ECC and CCL values and acceptable range of TARC, MEG values with high DG and gain.

ACKNOWLEDGMENT

The antenna measurement test facilities are supported by the Department of ECE, IIIT Naya Raipur. The authors are thankful to the HOD and the people in the Department of ECE, IIIT Raipur.

REFERENCES

1. Liu, Y., G. Xu, and X. Xu, "MIMO radar calibration and imagery for near-field scattering diagnosis," *IEEE Trans. Aerosp. Electron. Syst.*, Vol. 54, No. 1, 442–452, 2018.
2. Yegulalp, A. F., K. W. Forsythe, A. O. Hero, and D. W. Bliss, "Environmental issues for MIMO capacity," *IEEE Trans. Signal Process.*, Vol. 50, No. 9, 2128–2142, 2002.
3. Li, J. and P. Stoica, "MIMO radar with colocated antennas," *IEEE Signal Process. Mag.*, Vol. 24, No. 5, 106–114, Oct. 2007.
4. Yang, X., T. Zeng, C. Mao, C. Hu, and W. Tian, "Multi-static MIMO SAR three-dimensional deformation measurement system," *Proc. IEEE 5th Asia-Pacific Conf. Synth. Aperture Radar (APSAR)*, Vol. 1, 297–301, Singapore, 2015.
5. Haimovich, A. M., R. S. Blum, and L. J. Cimini, "MIMO radar with widely separated antennas," *IEEE Signal Process. Mag.*, Vol. 25, No. 1, 116–129, 2008.
6. Fishler, E., A. Haimovich, R. Blum, D. Chizhik, L. Cimini, and R. Valenzuela, "MIMO radar: An idea whose time has come," *Proc. the IEEE Radar*, 71–78, 2004.
7. Jayanthi, K. and A. M. Kalpana, "Mutual coupling reduction techniques between MIMO antennas for UWB applications," *International Journal on Recent and Innovation Trends in Computing and Communication*, Vol. 5, No. 9, 18–22, 2017
8. Shabbir, T., M. T. Islam, S. S. Al-bawri, R. W. aldhaheri, K. H. Alharbi, et al., "16-port non-planar MIMO antenna system with nzi metamaterial decoupling structure for 5G applications," *IEEE Access*, Vol. 8, 157946–157958, 2020.
9. Alibakhshikenari, M., B. S. Virdee, C. H. See, R. A. Abd-Alhameed, F. Falcone, et al., "Surface wave reduction in antenna arrays using metasurface inclusion for MIMO and SAR systems," *Radio Science*, Vol. 54, No. 11, 1067–1075, Nov. 2019, https://doi.org/10.1029/2019RS006871.
10. Mchbal, A., N. Amar Touhami, H. Elftouh, and A. Dkiouak, "Mutual coupling reduction using a protruded ground branch structure in a compact UWB Owl-shaped MIMO antenna," *International Journal of Ants. and Prop.*, Vol. 10, Article ID 4598527, 2018.
11. Wang, F., Z. Y. Duan, X. Wang, Q. Zhou, and Y. Gong, "High isolation millimetre-wave wideband MIMO antenna for 5G communication," *International Journal of Ants. and Prop.*, 1–12, 2019.
12. Kong, L. and X. Xu, "A compact dual-band dual-polarized microstrip antenna array for MIMO-SAR applications," *IEEE Trans. on Antennas and Prop.*, Vol. 66, No. 5, 2374–2381, 2018.

13. Feng, B., J. Lai, K. Chung, and Q. Zeng, "Dual-wideband and high-gain ME dipole antenna and its 3-D MIMO system with metasurface," *IEEE Access*, Vol. 6, 33387–33398, 2018.
14. Chen, Z., W. Zhou, and J. Hong, "Miniaturized MIMO antenna with triple band-notched characteristics for UWB applications," *IEEE Access*, Vol. 9, 63646–63655, 2021.
15. Al-bawri, S. S., M. T. Islam, G. Muhammad, M. D. Shabiul Islam, and H. Y. Wong, "Hexagonal shaped NZI MTM based MIMO antenna for mm-Wave application," *IEEE Access*, Vol. 8, 181003–181013, 2020.
16. Amin, F., R. Saleem, S. Ur Rehman, M. Bilal, M. F. Shafique, and T. Shabbir, "A compact quad-element UWB-MIMO antenna system with parasitic decoupling mechanism," *Appl. Sci.*, Vol. 9, 1–13, 2019.
17. Yin, C., Z. Li, and X. Zhu, "Compact UWB MIMO vivaldi antenna with dual band-notched characteristics," *IEEE Access*, Vol. 7, 38696–38701, 2019.
18. Xi, Z., Z. Tang, X. Wu, J. Znan, S. Hu, and Y. L. Xin, "Compact UWB-MIMO antenna with high isolation and triple band-notched characteristics," *IEEE Access*, Vol. 7, 19856–19865, 2019.
19. Kumar, P., S. Urooj, and A. Malibari, "Design and implementation of quad-element SWB MIMO antenna for IoT applications," *IEEE Access*, Vol. 8, 697–704, 2020.
20. Shabbir, T., R. Saleem, S. S. Al-Bawri, M. F. Shafique, and M. T. Islam, "Eight-port metamaterial loaded UWB-MIMO antenna system for 3D system-in-package applications," *IEEE Access*, Vol. 8, 106982–106992, 2020.
21. Iqbal, A., A. Basir, A. Smida, N. K. Mallat, I. Elfergani, et al., "Electromagnetic bandgap backed mm-Wave MIMO antenna for wearable applications," *IEEE Access*, Vol. 7, 111135–111144, 2019.
22. Molins-Benlliure, J., E. Antonino-Daviu, M. Cabedo-Fabrés, and M. Ferrando-Baller, "Four-port wide-band cavity-backed antenna with isolating X-shaped block," *IEEE Access*, Vol. 9, 80535–80545, 2021.
23. Jaglan, N., D. Kumar, S. D. Gupta, T. Ekta, B. K. Kanaujia, and S. Shweta, "Triple band notched mushroom and uniplanar EBG structures based UWB MIMO/diversity antenna with enhanced wideband isolation," *International Journal of Elens. and Coms.*, Vol. 90, 36–44, 2018.
24. Khan, A., S. Bashir, G. Salman, and K. Qureshi, "Mutual coupling reduction using ground stub and EBG in compact wideband MIMO-antenna," *IEEE Access*, Vol. 9, 40972–40979, 2021.
25. Alibakhshikenari, M., M. Khalily, B. S. Virdee, C. H. See, R. A. Abd-Alhameed, and E. Limiti, "Mutual coupling suppression between two closely placed microstrip patches," *IEEE Access*, Vol. 7, 23606–23614, 2019.
26. Elsharkawy, R. R., A. S. A. El-Hameed, and S. M. El-Nady, "Quad-port MIMO filtenna with high isolation employing BPF with high out-of-band rejection," *IEEE Access*, Vol. 10, 3814–3824, 2022.
27. Al-Bawri, S. S., Md S. Islam, H. Y. Wong, M. F. Jamlos, A. Narbudowicz, M. Jusoh, T. Sabapathy, et al., "Metamaterial cell-based superstrate towards bandwidth and gain enhancement of quad-band CPW-Fed antenna for wireless applications," *Sensors*, Vol. 20, 1–14, 2020.
28. Al-Bawri, S. S., H. H. Goh, Md S. Islam, H. Y. Wong, M. F. Jamlos, A. Narbudowicz, M. Jusoh, et al., "Compact ultra-wideband monopole antenna loaded with metamaterial," *Sensors*, Vol. 20, 1–15, 2020.
29. Arpan, D., P. Merch, K. Jayshri, G. Byun, and T. K. Nguyen, "Wideband flexible/transparent connected-ground MIMO antennas," *IEEE Access*, Vol. 9, 147003–147015, 2021.
30. Alibakhshikenari, M., F. Babaeian, B. S. Virdee, S. Aïssa, L. Azpilicueta, et al., "A comprehensive survey on "Various decoupling mechanisms with focus on metamaterial and metasurface principles applicable to SAR and MIMO antenna systems"," *IEEE Access*, Vol. 8, 192965–193004, 2020.
31. Ayman, A. A., "Low-interacted multiple antenna systems based on metasurface-inspired isolation approach for MIMO applications," *Arab. J. Sci. Eng.*, Vol. 47, 2629–2638, 2022.
32. Alibakhshikenar, M., B. S. Virdee, P. Shukla, C, H. See, R, A. Abd-Alhameed, et al., "Isolation enhancement of densely packed array antennas with periodic MTM-photonic bandgap for SAR and MIMO systems," *IET Microwaves, Antennas & Propagation*, Vol. 14, No. 3, 183–188, 2020.

33. Alibakhshikenar, M., B. S. Virdee, C. H. See, R. Abd-Alhameed, and F. Falcone, "Array antenna for synthetic aperture radar operating in X and Ku-bands: A study to enhance isolation between radiation elements," *EUSAR 2018; 12th European Conference on Synthetic Aperture Radar*, 1083–1087, 2018.
34. Alibakhshikenar, M., B. S. Virdee, P. Shukla, C. H. See, R. Abd-Alhameed, M. Khalily, et al., "Antenna mutual coupling suppression over wideband using embedded periphery slot for antenna arrays," *Electronics*, Vol. 7, No. 9, 198, 2018.
35. Alibakhshikenar, M., B. S. Virdee, C. H. See, R. Abd-Alhameed, and F. Falcone, "Interaction between closely packed array antenna elements using metasurface for applications such as MIMO systems and synthetic aperture radars," *Radio Science*, Vol. 53, 1368–1381, 2018.
36. Alibakhshikenar, M., B. S. Virdee, C. H. See, R. Abd-Alhameed, and F. Falcone, "A new study to suppress mutual-coupling between waveguide slot array antennas based on metasurface bulkhead for MIMO systems," *Proceedings of the 2018 Asia-Pacific Microwave Conf. (APMC)*, 500–502, 2018.
37. Alibakhshikenar, M., B. S. Virdee, C. H. See, R. Abd-Alhameed, and F. Falcone, "A new waveguide slot array antenna with high isolation and high antenna bandwidth operation on Ku- and K-bands for radar and MIMO systems," *Proceedings of the 48th European Microwave Conf. (EuMC)*, 1421–1424, 2018.
38. Alibakhshikenar, M., B. S. Virdee, C. H. See, R. Abd-Alhameed, and F. Falcone, et al., "Study on antenna mutual coupling suppression using integrated metasurface isolator for SAR and MIMO applications," *Proceedings of the 48th European Microwave Conf. (EuMC)*, 1425–1428, 2018.
39. Alibakhshikenar, M., M. Khalily, and B. S. Virdee, et al., "Mutual-coupling isolation using embedded metamaterial em bandgap decoupling slab for densely packed array antennas," *IEEE Access*, Vol. 7, 5182–51840, 2019.
40. Alibakhshikenar, M., M. Khalily, and B. S. Virdee, et al., "Mutual coupling suppression between two closely placed microstrip patches using EM-bandgap metamaterial fractal loading," *IEEE Access*, Vol. 7, 23606–23614, 2019.
41. Alibakhshikenar, M., B. S. Virdee, and E. Limiti, "A technique to suppress mutual coupling in densely packed antenna arrays using metamaterial supersubstrate," *12th European Conference on Antennas and Propagation*, 9–13, 2018.
42. Sunita, A. N. and B. Gauraw, "Design of squared shape SRR metamaterial by using rectangular microstrip patch antenna at 2.85 GHz," *4th International Conference on Signal Proc. and Integrated Ntrks (SPIN)*, 196–200, IEEE, 2017.
43. Kiruthika, R. and T. Shanmuganantham, "Comparison of different shapes in microstrip patch antenna for X-band applications," *International Conference on Emerging Technological Trends (ICETT)*, 1–6, Oct. 2016.
44. Khan, S. and T. F. Eibert, "A multifunctional metamaterial-based dual-band isotropic frequency-selective surface," *IEEE Trans. on Antennas and Prop.*, Vol. 66, No. 8, 4042–4051, 2018.
45. Saharawi, M. S., A. T. Hassan, and M. U. khan, "Correlation coefficient calculations for MIMO antenna systems: A comparative study," *International Journal of Microw. and Wireless Tech.*, 1–14, 2017.